Neuro-Oncology Advances

6(1), vdae064, 2024 | https://doi.org/10.1093/noajnl/vdae064 | Advance Access date 8 May 2024

A neural tract-inspired conduit for facile, on-demand biopsy of glioblastoma

Martha I. Betancur[†], Ayden Case[†], Ekaterina Ilich, Nalini Mehta, Sean Meehan, Sabrina Pogrebivsky, Stephen T. Keir, Kevin Stevenson, Barun Brahma, Simon Gregory, Wei Chen, David M. Ashley, Ravi Bellamkonda, and Nassir Mokarram

All author affiliations are listed at the end of the article

[†]These authors contributed equally to this work.

Corresponding Authors: Nassir Mokarram, PhD, Department of Neurosurgery, Emory University, 1365 Clifton Road NE, Suite B6200, Atlanta, GA 30322, USA (nassir.m@emory.edu); Ravi Bellamkonda, PhD, Biology, Emory University, 1518 Clifton Road, Atlanta, GA 30322, USA (ravi@emory.edu).

Abstract

Background. A major hurdle to effectively treating glioblastoma (GBM) patients is the lack of longitudinal information about tumor progression, evolution, and treatment response.

Methods. In this study, we report the use of a neural tract-inspired conduit containing aligned polymeric nanofibers (i.e., an aligned nanofiber device) to enable on-demand access to GBM tumors in 2 rodent models. Depending on the experiment, a humanized U87MG xenograft and/or F98-GFP+ syngeneic rat tumor model was chosen to test the safety and functionality of the device in providing continuous sampling access to the tumor and its microenvironment.

Results. The aligned nanofiber device was safe and provided a high quantity of quality genomic materials suitable for omics analyses and yielded a sufficient number of live cells for *in vitro* expansion and screening. Transcriptomic and genomic analyses demonstrated continuity between material extracted from the device and that of the primary, intracortical tumor (in the *in vivo* model).

Conclusions. The results establish the potential of this neural tract-inspired, aligned nanofiber device as an on-demand, safe, and minimally invasive access point, thus enabling rapid, high-throughput, longitudinal assessment of tumor and its microenvironment, ultimately leading to more informed clinical treatment strategies.

Key Points

- The neural tract-inspired aligned nanofiber device safely provides a preferred migration path for GBM in both animal models and can be easily accessed on-demand for longitudinal tumor sampling.
- Besides the tumor itself, tumor microenvironment is also present within the aligned nanofiber device in enough quantity and quality for downstream omics analyses.
- Live, culturable tumor cells can also be obtained to develop personalized treatments.

Finding an effective treatment for glioblastoma (GBM) has been challenging in part due to the lack of reliable and accurate means to longitudinally monitor the effect of therapies on tumor progression and evolution in a timely and frequent manner. The heterogeneity of this disease is mainly responsible for the unusually high rate of resistance and recurrence, representing the primary etiology of death in nearly all GBM patients.[1–3] Current standard of care imaging and biopsy modalities are severely limited in their ability to provide accurate longitudinal information about GBM, its microenvironment, and, ultimately, the effectiveness of a given treatment.[4,5] Magnetic resonance imaging (MRI) offers little insight into the cancer's molecular characteristics and progression,[6–8] while invasive tissue biopsies are performed infrequently and

Importance of the Study

Application of this device is poised to have a major impact on patient quality of life and treatment management by avoiding the need for frequent, invasive tissue biopsy while providing on-demand, relevant, and accurate data about the tumor. As GBM is a characteristically heterogenous disease, this on-demand, subcutaneously accessible sampling approach can significantly improve the effectiveness of clinical trials by providing longitudinal feedback for better patient stratification and monitoring, leading to more successful outcomes in treating this challenging disease.

in a limited capacity due to their inherent risk, and therefore are only able to provide a narrow, finite snapshot of the disease.[9] Emerging technologies such as liquid biopsy, which analyzes circulating tumor cells, have shown promise for monitoring other cancers but are inherently limited in surveying brain tumors due to the blocking nature of the blood–brain barrier (BBB),[9,10] which severely restricts availability of tumor material in accessible fluids, blood and cerebral spinal fluid (CSF).[9,11,12] Furthermore, there is a lag between the time tumor material can be detected in circulation and the evolving characteristics of the primary tumor site, resulting in uncertainty about continuity between the two.[13]

In order to develop a more effective therapy, it is essential to enable more frequent and accurate surveillance of the tumor and its microenvironment throughout the course of treatment. Longitudinally informed surveillance will also enable a more effective clinical trial design by matching GBM patients (who often have less than a year-long survival window after disease recurrence) with the most personalized approaches in a timely manner.[14,15] Therefore, providing a safe and reliable method of assessing GBM progression and treatment response over time would be a major step forward in managing this challenging disease.

In this article, an alternative approach to enable longitudinal and accurate monitoring of GBM tumors is described which exploits the invasive way that cancer cells utilize white matter tracts to migrate. We hypothesized that the neural tract-inspired device (consisting of an aligned nanofiber film inside a polymeric conduit) would enable on-demand access to tissue representative of the intracortical tumor through minimally invasive aspiration of the device's reservoir. To test this hypothesis, we (i) designed a biocompatible and clinically relevant device that guides tumor tissue to the device's proximal end; (ii) investigated the acute/subacute safety and functionality of this device in 3 different animal models; and (iii) evaluated device's ability to provide relevant information regarding the intracortical tumor.

Materials and Methods

Neural Tract-Inspired Conduit Description

The device tested in rats consisted of a conduit with an aligned nanofiber film placed longitudinally within the tube (Supplementary Figure 1). The film was composed of nanofibers that were generally aligned coaxially within the conduit. Eighty percent of fibers must have had a longitudinal orientation with an included angle of 20% or less. The average fiber diameter was 650 ± 150 nm and the film thickness ranged between 100 µm and 200 µm. These aligned fibers promoted the migration of tumor cells through the tube by mimicking the white matter tracts and blood vessels that physically guide the migration of GBM cells. Three different types of films were tested: smooth polycaprolactone (PCL), aligned PCL, and aligned aliphatic polyurethane (PU). This family of siloxane segmented polyurethanes has the mechanical properties of polyurethanes while exhibiting the biological stability of silicone rubbers. A total of 6 different iterations of the aligned nanofiber device and 4 control designs were tested in different experiments accordingly (see Supplementary Figure 1, Supplementary Tables 1 and 2). When longitudinally attached (to the diameter of the conduit), the film was stretched along the middle of the conduit with both parallel edges glued to the conduit in a longitudinal fashion. The "rolled in" or lumen design had the film attached to the conduit at only one end, with the other end not attached, but rolled inwardly at the center of the conduit.

The different films were assessed within 3 different conduit materials: PCL (made in house), PU, and silicone obtained from vendors (Figure 1A). PU conduits were selected as optimal conduits to be used for the on-demand biopsy sampling experiments. Each PU conduit had a length of 7–8 mm, an outer diameter of 2.6 mm, and an inner diameter of 1.8 mm. The catheters had an open distal end, with ~5–6 mm of the conduit protruding from the skull, mimicking the reservoir area, which would sit in the skull with the covered proximal end under the scalp in a clinical application.

Quality assurance was performed on devices before they were used for the rat studies. Devices were tested for sterility by direct inoculation of antibiotic-free media with randomly selected, finalized devices. Any capillary effect was minimized by pre-filling the devices with saline before implantation.

Chronic Rabbit Safety Study

A chronic implant study in rabbits, along with several other biocompatibility studies (Supplementary Figure 9, Supplementary Tables 8 and 9), was conducted by Wuxi Apptec and delegated test facilities, all ISO 17025 certified analytical laboratories. All tests were performed in general compliance with applicable domestic and international test standards per ISO 10993-11 and ISO 10993-6 Annex

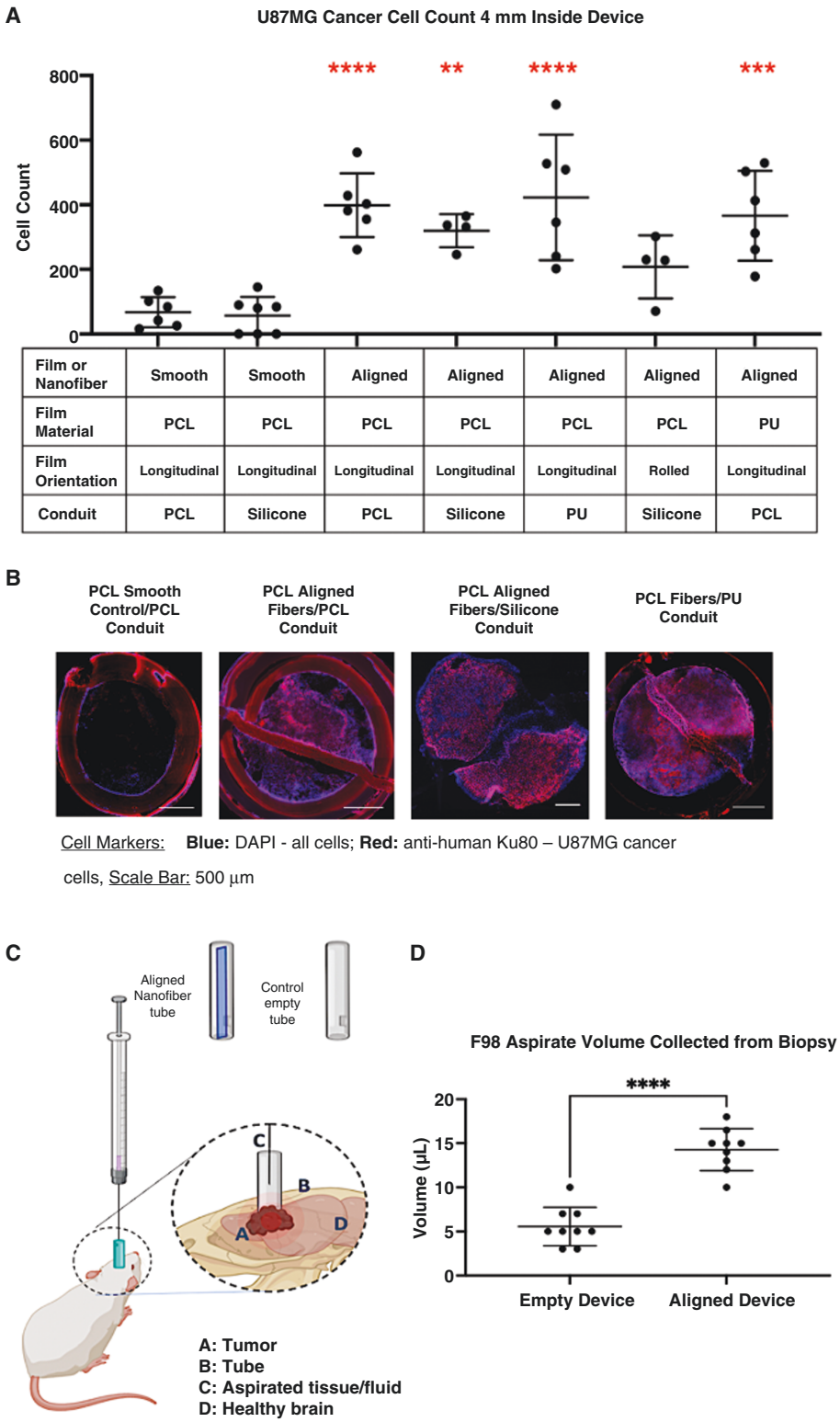

Figure 1. Aligned nanofiber topography guides cancer cells away from the tumor and toward the proximal end of the device which enables on-demand and minimally invasive access to tumor tissue, as demonstrated via histology and aspiration analyses. (A) Comparison of conduit and nanofiber materials in U87MG GBM rat model; all devices, except silicone/rolled aligned films, were attached to the tubing on both sides longitudinally to the cylindrical conduit. The aligned nanofiber film devices had significantly larger amounts of cells and tissue migrating toward the proximal end of device relative to the smooth film controls. (B) Histological evidence that cancer cells migrated to fill the entire length of implanted aligned device: immunofluorescent images of a transverse cross-sections of tissue at 4 mm from the proximal end of the devices showing tumor cells filling the aligned nanofiber devices. (C) Illustration of position of device relative to tumor and skull as well as the biopsy aspirate procedure. (D) Comparison of total aspirate volumes in the F98-GFP+ rat model between aligned nanofiber device and control empty device. ****$P < .0001$.

D as well as following Good Laboratory Practices (21 CFR Part 58). The article under test was the clinical version of the aligned nanofiber device, consisting of identical materials to the devices in other parts in this study. Devices for this portion of the study were manufactured and sterilized under lot control. A representative fragment of the test article or comparably sized and shaped High-Density Polyethylene (HDPE) control was gently placed on the brain parenchyma surface on the left or right hemisphere per animal. The dura was repaired and the dermal incisions were surgically closed. This test was designed to reveal toxicity or excessive fibrosis relative to the control due to the materials. Identical test articles were implanted on each side of midline subcutaneously for a total of 3 implants per animal. In total, 12 rabbits (6 males and 6 females) were implanted with the control article and 13 rabbits (7 males and 6 females) were implanted with the test article. Rabbit health was continuously observed including daily to weekly neurological and clinical assessment, and after 26 weeks of exposure to the implants, rabbits were sacrificed, and extensive histopathology was performed for assessment of local and systemic effects. Slides were prepared for immunohistochemistry using the following: H&E stain, Fluoro-jade stain (a marker for degenerating neurons); Luxol Fast Blue (LFB) stain (a marker for myelin); as well as anti-GFAP (glial fibrillary acidic protein as an astrocyte marker) and anti-Iba-1 (microglial and macrophage marker) (Supplementary Figure 9 and Supplementary Table 8). In addition to histological examination, whole blood was collected at termination and plasma was harvested from it. Each sample was then analyzed accordingly for different parameters related to acute and systemic toxicity, listed in Supplementary Table 9.

Cell Culture

F98 glioma cells were transduced with a lentiviral vector to express Green Fluorescent Protein (GFP) and implanted at 2000 cells/µl in phosphate buffered saline (PBS). U87MG human GBM cells were expanded and collected for inoculation at a concentration of 100,000 cells/µl.

Tumor Inoculation

All procedures were approved by Duke University Institutional Animal Care and Use Committees (IACUC) under protocol #A245-19-11.

RNU nude male rats (125–175 g, Charles River Laboratories) were inoculated with 500,000 U87MG human glioma cells per rat. Fisher (CDF) male rats (10–11 weeks old, Charles River Laboratories) were inoculated with 10,000 F98 GFP+ rat glioma cells per animal.

Animals were induced using between 2% and 5% isoflurane. Subcutaneous Buprenorphine Extended Release (Bup-ER) injections were given before each surgical procedure. A ~2 cm incision was made to reveal bregma on skull. Bupivacaine was given at the incision site. A craniotomy at 2 mm lateral and 2 mm posterior from bregma was performed, followed by needle insertion 2 mm deep into the brain. Intracortical inoculation of the specified cell type at the desired concentration in 5 µl of saline at a rate of 1 µl/min was initiated. The craniotomy was covered with bone wax and the skin was sutured.

A systematic method was developed to prevent tumors from growing onto the scalp, which involved a combination of injection timing, wait time to remove the needle, immediate addition of bone wax to the burr hole, and cleaning of the injection area after treatment.

MRI Visualization

Seven to 8 days post-inoculation and 11–15 days (for U87MG) and 9–12 days (for F98) post-device implantation, animals underwent a MR Imaging study to assess the success of tumor inoculation and to evaluate tumor growth and migration (see Supplementary Figure 2 for timeline). Animals were imaged using a 7 Tesla (7T) Bruker Biospec small animal magnetic resonance (MR) scanner (Bruker Inc., Billerica, MA), utilizing a receive-only 4-coil array combined with a 72 mm volume coil for transmission. Animals were anesthetized using 5% isoflurane to induce and then maintained at 2% isoflurane during imaging. To obtain T2-weighted images, the following parameters were used for axial 2D RARE images of brain and scaffold: 5.7 s repetition time; 45 ms echo time; in-plane field of view (FOV) of 2.8 cm × 2.8 cm; slice thickness of 0.5 mm over 40 slices. Approximately 9 days after device implantation, animals underwent a second, identical MRI study to confirm effective and uniform placement of the device. MR images of the device contents and surroundings were evaluated for noninvasive indications of tissue interaction with the device. MR images were rendered, and tumor volumes were calculated using the 3D Slicer image computing platform (slicer.org). Subjects with no visible evidence of tumor from MRI or necropsy analysis were removed from the study.

Device Implantation

One day after the first MRI, animals were anesthetized and treated with analgesics, as described above. Animals were assigned to different device implant groups 7–8 days post-inoculation. For both studies, animals were placed into different groups using the tumor sizes observed under MRI prior to implantation to ensure that the average initial tumor size of each group was similar. Animals in the U87MG experiment were implanted with the PU conduit combined with the PU aligned nanofiber device ($n = 8$), a smooth film device (control) ($n = 9$), a device with an aligned nanofiber ($n = 6$), or not implanted at all ($n = 10$). Animals in the F98-GFP+ experiment were implanted with an empty device (control) ($n = 9$), a device with an aligned nanofiber ($n = 8$), or not implanted at all ($n = 7$) (see Supplementary Tables 1 and 2).

For all implants, a 2.5–2.9 mm craniotomy was drilled at the location of tumor inoculation. The dura was ruptured to implant the device approximately 1.5–2 mm deep into the brain. An outer tube, with a diameter larger than that of the craniotomy, sat on the skull surrounding the implanted device to provide stability to the reservoir area. A Tegaderm membrane was used to cover the proximal end of the device, and dental cement was used to secure the device to

the skull. The skin was sutured to enclose the device completely. The animals recovered under a heat lamp before being returned to their housing areas.

Biopsy and Sample Acquisition and Preparation

A pilot feasibility test of on-demand, longitudinal access for sampling was performed with 3 F98-GFP+ and 3 U87MG inoculated rats which were biopsied several times after device implantation. Each group had 1 rat that received the control device and 2 were implanted with aligned nanofiber devices. Minimally invasive biopsies were performed through the proximal end of the device, which was accessible through a small incision in the skin. Biopsies were obtained 2, 4, and 6 days after device implantation and samples were evaluated for volume obtained from reservoir and signs of infection. The skin was sutured after the first 2 biopsies and animals were left to recover. After the third biopsy, the animals were sacrificed. All samples underwent mechanical dissociation at least once for cell isolation. Samples made up of dense tissue-like material required repeated mechanical dissociation. Once cells were isolated and diluted, trypan blue staining was used to manually count the live cell content in each sample (Supplementary Table 3). To identify tumor cell ratio to other cells, such as immune cells, each sample was divided into 4 equal portions and immunostained using 4 different flow cytometry panels.

Animals used for the genomic analysis were biopsied through the proximal end of the device, perfused, and euthanized either when they reached humane endpoint or at the predetermined endpoint (no more than a 4-day difference), whichever came first. To obtain information about the tumor and its microenvironment, the syngeneic F98-GFP+ model animals were biopsied once after being given Bup-ER analgesic. While under deep isoflurane anesthesia, a small incision was made on the skin atop the device region. A small piece of dental cement atop of the device was clipped off, and the Tegaderm membrane covering the proximal end of device was removed. First, fluid was aspirated from the implanted device using a 26-gauge needle. The amount and physical appearance of biopsied samples were measured and noted. Each animal was then placed under deeper general anesthesia and euthanized via cardiac perfusion with PBS. Implanted devices were then carefully dissected, and tumor tissue was separated from the brain. For animals marked for transcriptomic analysis, the entire device and samples from healthy brain tissue were stored for later analysis in RNALater solution. For animals selected for histology, the entire brain and the device implanted within it were dissected, submerged in OCT, and frozen in liquid nitrogen.

Nucleic Acid/Genomic Analysis

DNA and RNA from the aspirate, tissue recovered from within the implanted device, tumor tissue biopsy, and brain tissue biopsy from each animal were extracted and the quantity and quality of each assessed using Qubit (Invitrogen) analysis. DNA was extracted using Thermofischer Pure Link Genomic Extraction Kit (cat. #K1820). RNA was extracted using Qiagen RNeasy Plus Mini Kit (cat. #74134).

DNA library preparation was performed using a KAPA HyperPrep Kit (Roche). For the RNA library preparation, the KAPA Stranded mRNA-Seq Kit (Roche) was used. Library quality control and quantification were performed using the QuBit DNA HS Assay (ThermoFisher) and the HS NGS Fragment (1–6000 bp) Assay (Agilent). Bulk RNA and DNA sequencing were performed by Duke University's Genomic Core Facility using a standard Illumina sequencing workflow using a NovaSeq 6000 SP flow cell at 100 bp PE. Downstream data analysis including CIBERSORTx and differential gene expression were performed by the Duke University's Genomic Core Facility.

The Whole Genome Sequencing experiment and data analysis were also performed by Duke University's Genomic Core Facility (Supplementary Figure 5).

Cell Culture of Biopsied Samples

Aspirate retrieved from the implanted device was added to tumor growth media, then transported to tissue culture. Under sterile conditions, the larger tissue pieces obtained from the aligned device were broken down using mechanical disruption and filtration methods of cell dissociation. The cells were then transferred into a 25 cm^2 tissue culture flask which was incubated at 37°C in a 5% CO_2 incubator. After cells had time to attach overnight, cells were imaged, expanded into larger flasks as needed and, after a week, cells were manually counted using a hemocytometer.

Histological Analysis and Immunohistochemical (IHC) Analysis

Frozen brain tissue and devices were cryosectioned horizontally into 30 µm-thick sections for different device evaluation in the U87MG xenograft study, and coronally into 12 µm-thick sections for the F98-GFP+ biopsy study. Slides were fixed with ethanol and prepared for histological analysis as previously described[16] using antibodies referenced in Supplementary Table 7. Tiled images were obtained using a Leica semi-confocal microscope fluorescent imaging system, and quantification procedures were performed for DAPI, GFP, and Ku80 antibodies using pre-defined thresholds. Images were processed through either Image J or MetaMorph Microscopy Image Analysis Software.

Statistical Analysis and Other Software

Data are presented as mean ± SD. Statistical analysis results and graphs were obtained using GraphPad Prism Version 9.3.1. Unpaired *t*-tests were performed for statistical analysis of data comparing 2 groups. For comparisons of 3 or more groups, 1-way ANOVA with Dunnett's or Sidak's multiple comparison test was used. For comparison of change in individual tumors, 2-way ANOVA or Sidak's multiple comparison test was performed on MRI tumor volumes. Illustrations of brain and devices were done using Sketchbook, Inc., Software.

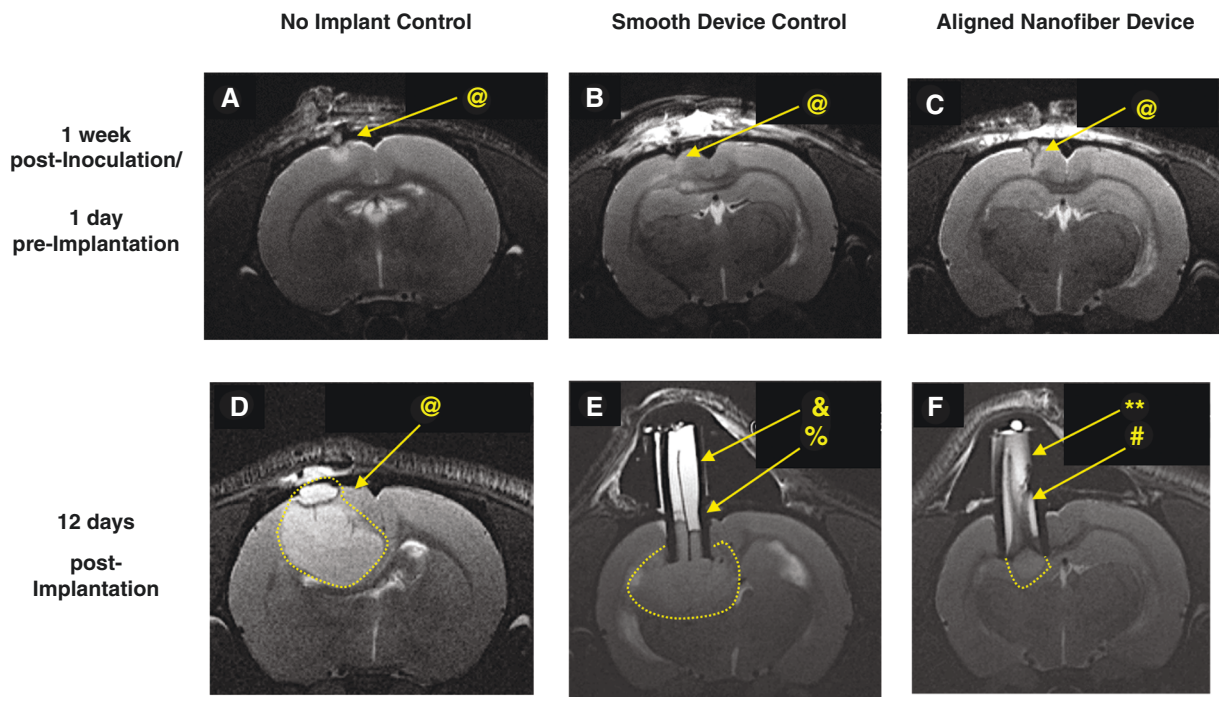

Figure 2. Representative T2-weighted MR images of U87MG model pre- and post- device implantation showing no adverse response to implant while confirming the possibility of noninvasive monitoring of tissue migration inside the device. (@: tumor, &: fluid, %: edge, **: flow voids, #: gradient). One week post-inoculation: (A) no implant control, (B) smooth film device control, (C) aligned nanofiber device. 12 days post-device implantation, (D) no implant control, (E) smooth film device control, and (F) aligned nanofiber device. In D, E, and F, tumor is surrounded by dotted white lines, bright white content inside device is fluid, and tissue inside device appears in gray tones. In (E), separation between tissue (gray) and fluid (white) is outlined by a dark edge between the two (%). Smooth film appears as a dark line at the center. In (F), inside the aligned nanofiber device, gray strips indicative of tissue appears along almost the entire length of device, and there is no well-defined edge separating the fluid inside the device from tumor. Flow voids (**) indicating interactions between tissue and fluid inside the aligned nanofiber device are visible.

GLP Quality Management

Implant studies involving F98 cells implemented quality management measures to ensure data integrity and comply with Good Laboratory Practice (GLP) to the extent possible according to 21 CFR Part 58, GLP for nonclinical laboratory studies guidelines (outlined within Supplementary Material).

Results

Aligned Topography is a Major Cue for Guiding Tumor Cells to the Reservoir

In vivo analyses in rodent models show that, regardless of the conduit material (PU, Silicone, or PCL), or nanofiber chemistry (PU or PCL), the greatest tissue migration was observed when aligned nanofibers were presented (Figure 1). This validates previous observations that orientation of nanofibers, more than their chemical characteristics, plays a role in guiding tumor migration (demonstrated in Supplementary Figure 6).[16] Thus, the topography of the aligned nanofibers provides the tumor with sufficient directional migration cues for cells to advance a significant distance away from tumor (Figure 1A and B). In fact, the volume of collected aspirate in the F98-GFP+ model (Figure 1C and D) and MRI evidence from the U87MG model (Figure 2) confirm the more robust migration of tissue with the aligned nanofiber device relative to smooth film or empty device control groups.

Following histological analyses, noninvasive evaluation of aligned nanofiber/tissue interaction was also performed using T2-weighted MR images (Figure 2 and Supplementary Figure 3). MRI images of the coronal view at the transverse end of implanted device were used to make detailed observations regarding the content inside devices and draw comparisons between aligned nanofiber devices, smooth film control devices, (Figure 2) and control empty devices (Supplementary Figure 3). Differences in delineation of tissue can be observed between the groups, with minimal tissue separation observed in the aligned nanofiber group, and clear tissue separation and fluid accumulation in the control empty devices outlined by sharp contrast in both tumor models (see fluid and edge labels on Supplementary Figure 3C, Figure 2D). While images of the aligned nanofiber devices indicate strong tissue presence throughout the length of the device, (Figure 2F, Supplementary Figure 3B), an overall homogenous, higher intensity appearance inside the control devices indicates stagnated fluid and no tissue migration inside the conduit (Figure 2E, Supplementary Figure 3C). This was

later validated by the presence of homogenous, translucent fluid collected during biopsies. Moreover, dark flow voids, observed only in aligned nanofiber devices, are indicators of dynamic interactions between tissue and liquid, and are associated with flowing fluids.[17–20] Overall the MRI data indicate that interactions between the nanofiber and GBM as well as the extent of tumor tissue migration can be monitored and confirmed noninvasively (Figure 2F, Supplementary Figure S3B).

Neural Tract-Inspired Aligned Nanofiber Device Does Not Cause Systemic Toxicity Nor Detrimentally Affect Survival

Although the aligned nanofiber device, which is comprised of a polyurethane (PU) conduit with PU aligned nanofibers, has a documented history of biocompatibility, we independently tested its acute, subacute, and chronic safety and neuro-biocompatibility in multiple relevant animal models.[21] Where applicable, the following controls were included: a PU conduit with a smooth PU film, an empty PU conduit, and no implant as additional controls. Animals receiving the aligned nanofiber device and control implants were closely monitored for changes in key vital signs and general indicators of malaise. Acute and sub-acute safety of the neural tract-inspired aligned nanofiber device were confirmed by imaging and monitoring physiological factors in both F98-GFP+ and U87MG rat tumor models. MRIs after implant showed no visible hemorrhage, edema, scarring, or inflammation in either tumor models nearly 2 weeks after implantation (Figure 2). The device remained fixed and tightly sealed at the site of implantation with no sign of infection observed in any of the subjects (Figure 2E,F, Supplementary Figure 3B and C). These same images show that in both GBM models the tissue in direct contact with the device appeared to heal properly, with little to no sign of inflammation, which can be visualized as bright intensity in T2-weighted MRIs.[20] By evaluating the tumor and device implants noninvasively and invasively, it was observed that none of the tested animals developed ectopic tumors, nor were there any signs that the tumor grew outside of the skull. Furthermore, none of the animals biopsied at multiple timepoints showed any signs of infection.

Moreover, sub-chronic and chronic safety of the aligned nanofiber device were also evaluated using neuron degeneration and gliosis markers along with whole blood analysis in the rabbit parenchyma models (Supplementary Figure 9). Overall, all measured parameters indicated there is no overall evidence of local or systemic toxicity due to the aligned nanofiber device. There were also no significant differences in body weight or feed consumption throughout the study, and hematological results were all within normal ranges (Supplementary Tables 8 and 9). There were statistically significant differences in male gamma-glutamyl transferase and female albumin levels throughout the study, but these were within biologically normal ranges. Histopathological and immunohistochemical observation both indicated that there were no specific adverse toxicological findings in the tissues examined that could be associated with systemic toxicity (Supplementary Figure 9). Therefore, the materials the aligned nanofiber device consist of are nonirritant and safe for chronic implantation.

Aligned Nanofiber Device Does Not Exacerbate Tumor Growth

Intracortical tumor volumes were compared to evaluate devices' effects on tumor growth, and both pre- and post-implantation tumor volumes were used to calculate tumor volume and change in intracortical tumor size over time (Figure 3A–D). Almost 2 weeks after implantation, MR images showed that devices did not cause an increase in intracortical tumor size greater than that seen in both controls in both U87MG and F98-GFP+ models. Furthermore, while animals in both tumor models implanted with the control device experienced significant changes in tumor volume when compared to their pre-implantation tumor volumes, in the U87MG model, post-implantation tumor volumes for the aligned group were not significantly different from their initially measured tumor volumes (Figure 3A). Thus, the aligned nanofiber group in the U87MG model demonstrated a significantly lower rate of change in intracortical tumor volume than that observed in the two control groups (Figure 3B). These significant differences between the aligned nanofiber group and the control groups, however, were not present in the F98-GFP+ model. In this syngeneic model, the aligned nanofiber devices and the control devices both experienced statistical significant in the intracortical tumor growth between the pre-implantation and post-implantation timepoints (Figure 3C). There was no difference in rate of change of intracortical tumor volume between the aligned nanofiber device and the controls (Figure 3D).

Most animals reached euthanasia end points within 17–21 days post-inoculation in the F98-GFP+ model. In the U87MG model, most animals survived between 28- and 35-days post-inoculation, with an exception noted for 3 animals in the aligned nanofiber device group and one animal in the no implant control group that survived over 100 days post-inoculation (Supplementary Figure 8). All results indicate that aligned nanofiber device does not pose a safety issue by exacerbating tumor growth in these rodent models.

Aligned Nanofiber Devices Can Be Used for Longitudinal, Minimally Invasive Tumor Access and Sampling

To mimic the application of this device in a clinical outpatient setting, the proximal end of the device (which sits well outside of the skull) was accessed and aspirated in a minimally invasive way 3 times per animal in a pilot test (Supplementary Table 3), then once in a final study to obtain sufficient samples for several relevant downstream analyses. The pilot biopsy experiment showed a trend of larger volumes and larger cell counts obtained from the aligned nanofiber devices among a series of biopsy samples in both GBM models. It also demonstrated that 2, 4, and 6 days were not the optimal time to obtain sufficient cells for extensive cell content analysis (Supplementary Table 3). This, along with the previous experiment on the

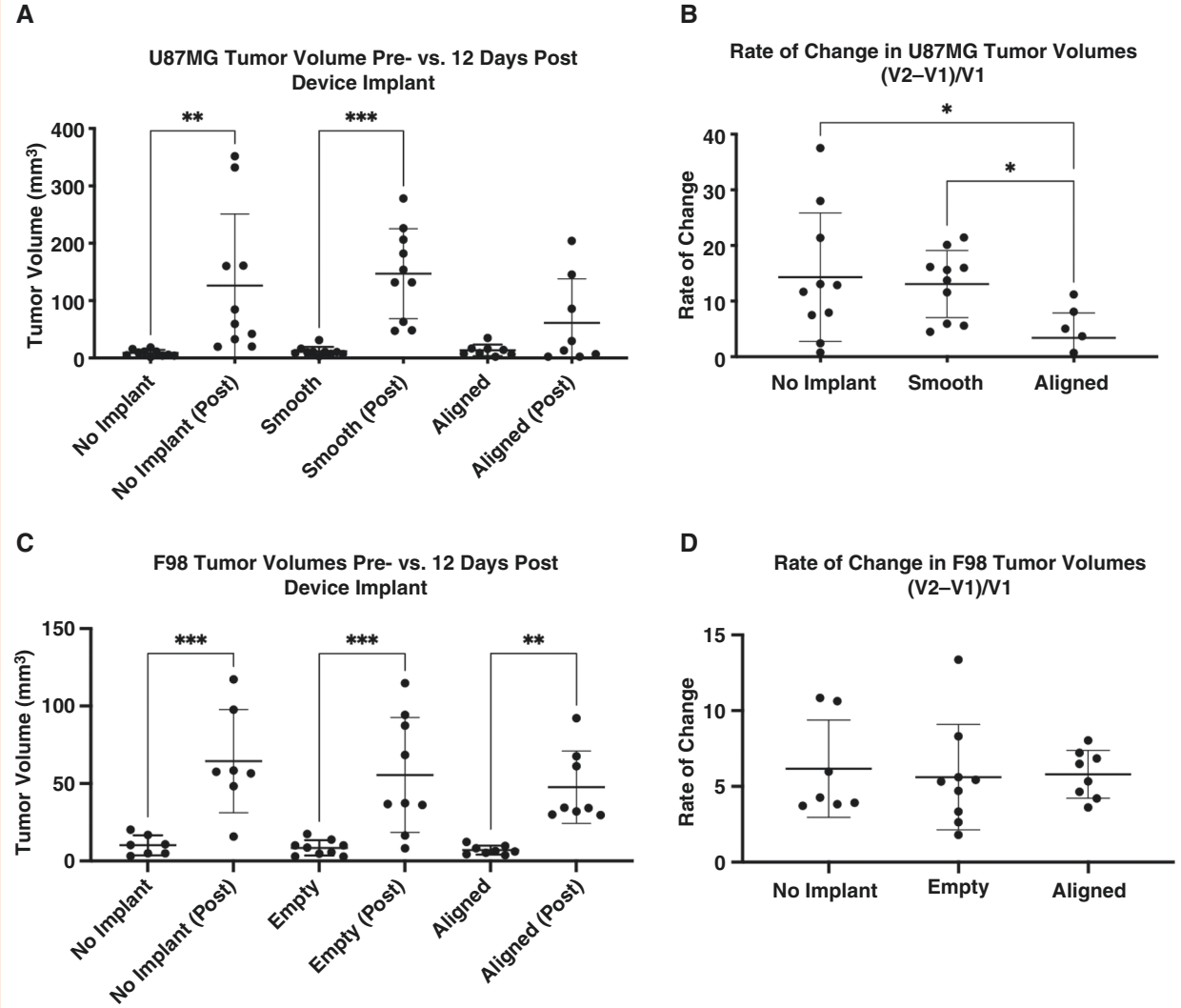

Figure 3. Tumor volumes in U87MG xenograft and F98 models. (A) No significant difference in U87MG tumor volumes post-implantation was observed between different groups. When initial volume is compared to final volume for each group, only the 2 control groups show significant growth of tumors in the U87MG model. (B) The significantly lower rate of change in tumor growth in aligned-implanted tumors indicates that, when U87MG cells migrate, intracortical growth is halted to an extent. (C) and (D) All 3 groups experience a significant growth with relatively similar rate of growth in F98 model. No Implant: No device implanted; Aligned: silicone/PU conduit with PU aligned nanofiber device implanted; Smooth: silicone/PU conduit with PU smooth film device implanted; Empty: empty silicone/PU conduit device implanted.

less aggressive xenograft model, in which devices were collected after 8–15 days, helped determine that the optimal first time point for a biopsy is between 8 and 12 days post-implantation, ensuring that sufficient viable cells would be collected. In addition, it was determined that the syngeneic GBM model was most appropriate to evaluate noncancer cells, particularly infiltrating immune cells.

The single biopsy experiment, collected between Day 9 and 12 post-implantation, had a significantly greater volume of tissue obtained from the aligned nanofiber device group relative to the control empty device group in an F98-GFP+ tumor model. This data points to a greater migration of cancer cells inside the device due to the aligned topography (Figure 1D). In addition to a larger aspirated volume, the aligned nanofiber device aspirates had greater viscosity than those obtained from empty devices, indicating a richer presence of solid tissue as opposed to physiological fluid. MRIs obtained from aligned devices showed also a convex-shaped proximal end that could be noninvasive indications of full tissue migration and pressure on the proximal end of the aligned nanofiber devices (Supplementary Figure 3B).

Tumor Microenvironment is Present Within the Aligned Nanofiber Device

In addition to facilitating access to migrating tumor tissue, the aligned nanofiber device can also facilitate direct sampling of the tumor microenvironment, including immune cells that are typically present within the tumor. Cellular and genomic analyses confirmed that cells composing the

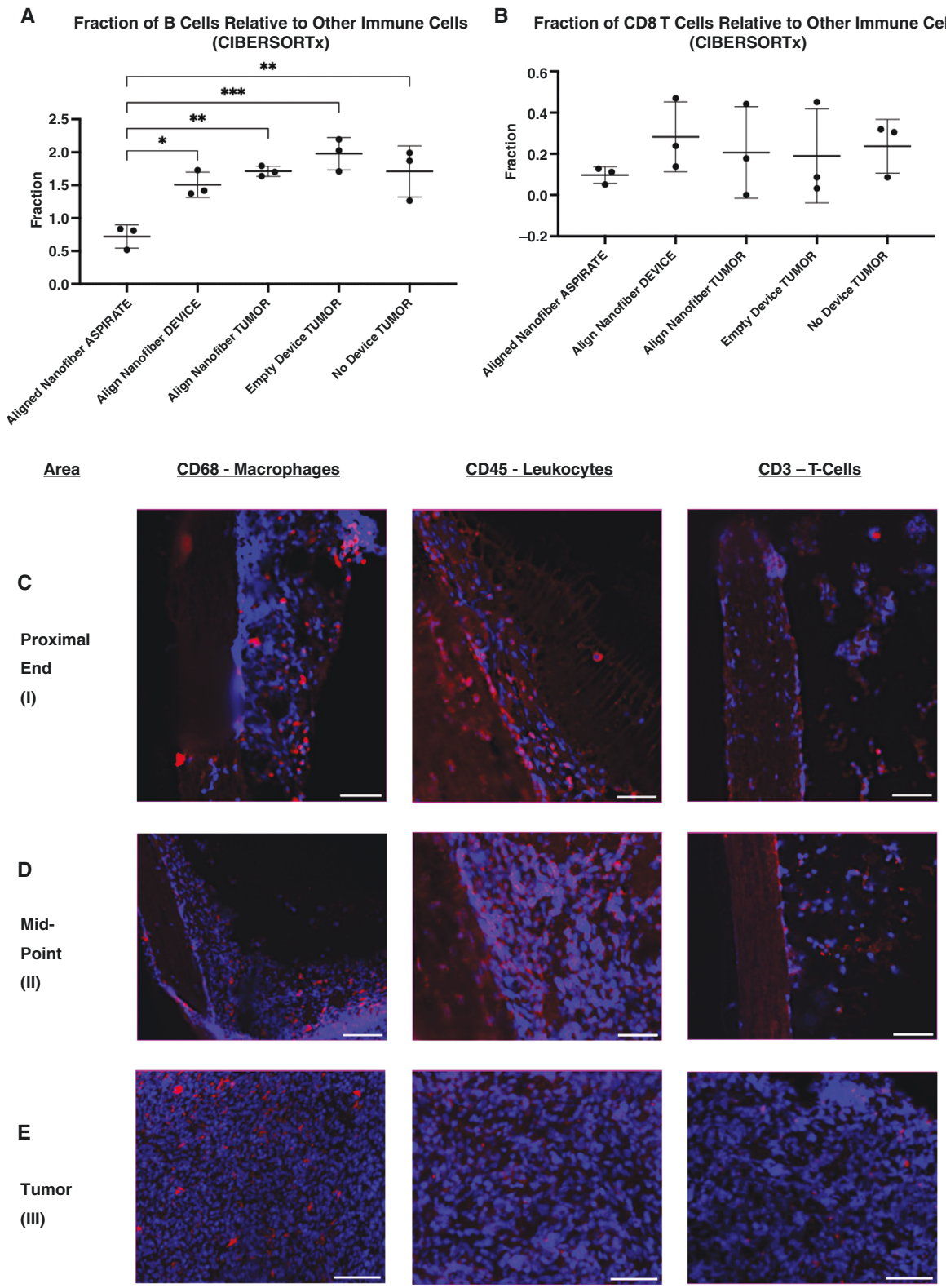

Figure 4. CIBERSORTx and IHC analyses of devices in F98-GFP+ tumor model. (A) and (B) CIBERSORTx analysis of bulk RNA-sequencing data for samples collected from: aspirated material from inside the aligned nanofiber device, tissue attached to the aligned nanofiber film within the device conduit, the intracortical tumor in the implant and control groups, and healthy brain tissue in the F98-GFP+ tumor model. (C)–(E). Aligned nanofiber devices retrieved after aspirate biopsy, sectioned transversely, stained, and imaged showing residual tissue that remained attached to the nanofiber. Within this adherent tissue, immune cells are present throughout the length of device. (C) (proximal end of device), (D) (midpoint of device), (E) (primary tumor mass) (scale bar: 50 μm). Blue: DAPI, Red: Immune Cell Marker.

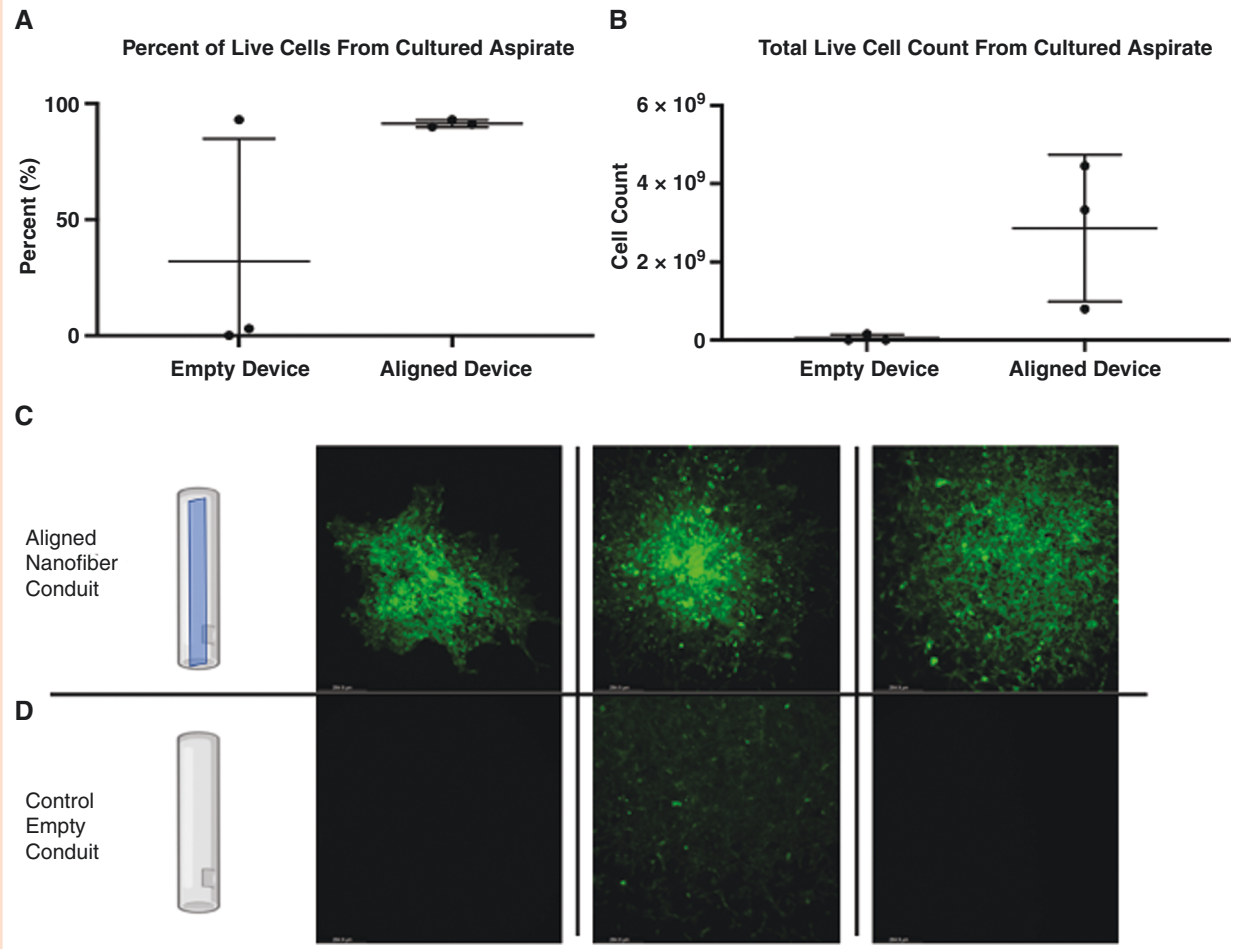

Figure 5. Cell culture from biopsy of F98-GFP+ tumor model. (A) Percentage of live cells in the culture expanded from biopsy aspirates of aligned nanofiber and control groups. (B) Absolute number of live cells in culture expanded for 7 days from biopsy aspirates of aligned nanofiber and control groups. (C) and (D) Representative images of the expanded culture after 1 week showing F98-GFP+ cells in all 3 of aspirates from aligned nanofiber devices and only a few GFP+ cells in one of the control empty devices.

tumor microenvironment are found throughout aligned nanofiber device alongside the tumor cells that migrated into the device (Figures 4 and 5). Quality analysis concluded that the material obtained from the aspirate of the control empty device and/or from the tissue within the control empty device did not have sufficient quantity and quality for omics analyses, therefore they were not processed (Supplementary Tables 4 and 5). Accordingly, only the tumor tissue obtained from the brain was analyzed for the empty devices as a control. Based on data obtained from bulk-RNA sequencing, key immune cells were found in tissue attached to the entire enclosed nanofiber device, as well as in the tissue/fluid aspirate from the proximal end of device (Figure 4A and B, Supplementary Figure 4). Bulk-RNA seq. data was processed using CIBERSORTx to determine immune-related differential gene expression within each sample.[22] Four different immune cell types were targeted: B cells, CD4+ and CD8+ T cells, and Natural Killer (NK) cells. Comparison of samples from tumor bulk, nanofiber device, control empty device, and no device control groups was conducted. Abundance ratios were determined by evaluating the expression level of more granular innate and adaptive immune cell-specific genes relative to the total leukocyte population.[22] No significant difference between abundance ratios of these cells between sampling location was found, except for the B cells respective to aspirate from the device (Figure 4, Supplementary Figure 4).

In addition to RNA sequencing, the presence of immune cells within the device was confirmed using immunohistochemistry (IHC) (Figure 4C–E). Aligned nanofiber devices were retrieved following biopsy, flash frozen in OCT, sectioned coronally, and processed for IHC. Results of this analysis corroborated the transcriptomic results generated via CIBERSORTx. Residual immune cell markers were observed both at the distal and proximal ends of the device after tissue/fluid biopsy was performed (Figure 4C–E).

Whole genome sequencing was performed for 3 animals; these results serve as a proof of concept, demonstrating that genomic analysis is feasible using material from the aligned nanofiber device (Supplementary Figure 5).

Live, Culturable Tumor Cells Can Be Obtained Proximally

Aligned nanofiber devices guided a sufficient number of tumor cells into the device conduit, making them easily accessible proximally and outside of skull for aspiration (Figures 1, 4, and 5). The ability to collect and culture these cells from the device was assessed ex vivo. Figure 5 illustrates that while a limited aspirate volume from the empty devices did not yield to any meaningful cell culture expansion, aspirated cells from aligned devices could be subsequently cultured and expanded. Moreover, most of the devices in the aligned nanofiber group presented with resistance to aspiration with a 26-gauge Hamilton syringe at the rate of approximately 1 µl/20 s. This tangible resistance to aspiration along with the cloudier and more heterogenous appearance of the aspirate obtained from aligned nanofiber devices indicated a presence of more abundant cellular content within the aligned nanofiber device group. These observations correspond with noninvasive observations made via MRI, which indicated an increased abundance of infiltrated tumor cells and tissue within aligned devices (Supplementary Figure 3B). In contrast, the more translucent, easily aspirated, and homogenous liquid obtained from empty devices correlated well to the bright, homogenous intensity (indicative of stagnated fluid and not cellular tissue) seen inside empty devices via MRI (Supplementary Figure 3C).

The number of GFP+ F98 cells cultured from the aspirate was assessed after 1 week of expansion. Both percentage of live cells to total cells and absolute number of live cells were higher in the aspirate from the aligned nanofiber group (Figure 5A and B). Cultures were visualized under fluorescence to assess distribution and density of GFP+ cells. Aligned nanofiber device aspirates demonstrated a more concentrated cell density and greater observable cell count when compared to empty device aspirates (Figure 5C and D).

Enough Quantity and Quality of Genomic Material Is Obtainable

Sampling via the aligned nanofiber device did not cause any detectable degradation in the DNA sampled from the aspirate. DNA A260/280 and A260/230 ratios were assessed, with the aligned nanofiber device yielding higher purity of genomic material on average (Supplementary Table 4). DNA yield however was not significantly different between the aligned nanofiber device and control (Figure 6A and B).

However, additional aspirate volume and tissue infiltration within the aligned nanofiber device did yield a greater quantity of RNA than the control empty device. Unlike the liquid obtained from the empty devices, the material obtained from aligned nanofiber devices was sufficient for subsequent transcriptomics (RNA-seq.) (Figure 6C and D) and whole genome sequencing (WGS) (Supplementary Figure 5). The RNA from the aligned nanofiber device was of higher quality, on average than the empty device as measured by RIN and %DV200 (Supplementary Table 5).

These results indicate that the aligned nanofiber device produces an advantage for increasing RNA yield in both aspirate and device-adherent material sampling. Overall, the aligned nanofiber device produced high quality DNA and RNA, and, in certain circumstances, provided a decisive advantage over an empty device.

Discussion

A recent publication by several of the Society for Neuro-Oncology investigators has highlighted the importance of serial tissue sampling to correct the drug development paradigm for glioblastoma.[23] This is in addition to several contemporary letters and trials suggesting the increased need for on-demand sampling in GBM.[24–27] In fact, the ability to continuously and frequently monitor other solid and heterogeneously evolving tumors (eg, epithelial ovarian cancer) has provided clinical benefits in the form of more informed (and effective) treatment plans, and improved median overall survival.[28,29] The emerging liquid biopsy approach, while showing promise for tumor sequencing and early-stage detection,[30,31] is currently limited to use as a correlative tool alongside traditional biopsy, mostly due to the scarcity of brain tumor material available in blood and CSF.[9,13] This means that the sensitivity required to find and evaluate the minimal amount of useful material will be prohibitively high.[32] Furthermore, there is a delay between the tumor material that can be detected in circulation and the tumor itself resulting in uncertainty about continuity between the two.[13] However, despite these limitations, there is significant ongoing interest in the field of liquid biopsy for brain tumors,[33] again attesting to the importance of repeated and longitudinal surveillance of GBM.

Given the insufficiency of liquid biopsies, multiple invasive tissue biopsies are required to adequately evaluate the cancer's changing, heterogenous progression and response to treatment.[23] In addition, the feasibility of using novel and promising protocols such as intratumoral microdialysis faces major challenges in overcoming the BBB's barrier functions.[34] With the efficiency and safety of microdialysis sample retrieval restricting it to a maximum of 10 days sampling,[35] it has become evident that a more robust, long-term approach is needed to improve on these techniques.

While devices such as the Ommaya Reservoir system were key inspiration for our aligned nanofiber device, a key advantage of the neural tract-inspired conduit is in its ability to provide direct tissue/cellular samples from the tumor and not the CSF or blood. To obtain sufficient tumor tissue and fluid from the conduit, the tumor and its microenvironment need to actively migrate onto the substrate (aligned nanofibers in this case) away from the tumor and towards the proximal end of device (ie, reservoir). Our previous study has shown that aligned polycaprolactone (PCL) nanofibers that mimic aligned neural tracts are effective in guiding tumor cells away from the tumor and even causing a shrinkage in the size of the tumor.[16] However, PCL exhibits a slow degradation profile and is not desirable for a long-term brain implant.[36] PU nanofiber, with a long history of documented neuro-compatibility, is the

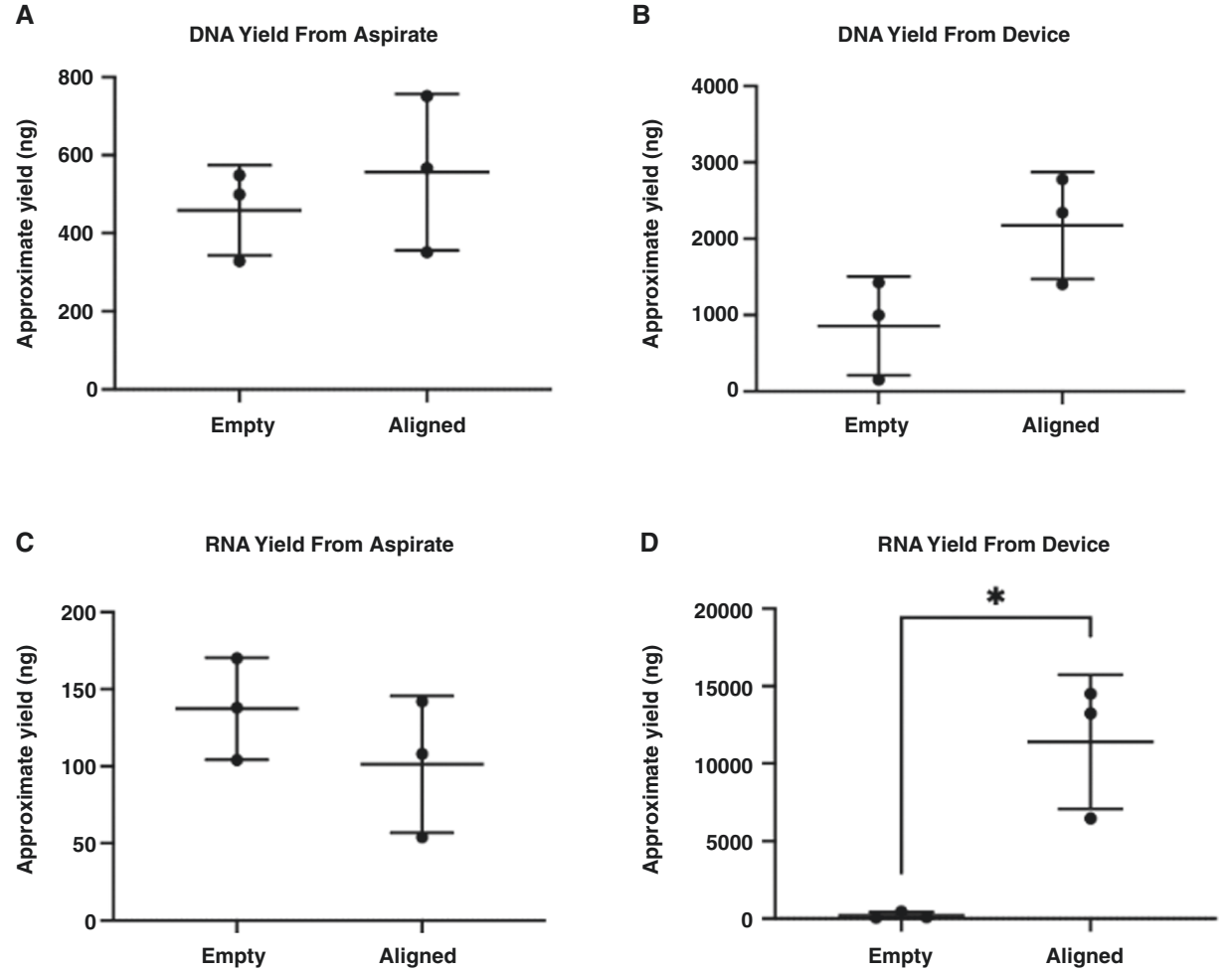

Figure 6. Genomic analysis of F98-GFP+ model. (A) and (B) Aspirate DNA yield and adherent material DNA yield for aligned nanofiber device and control empty device. (C) and (D) Aspirate RNA yield and adherent material RNA yield for aligned nanofiber device and control empty device.

best alternative that would enable potential clinical translation of this on-demand sampling device.[21,37–42]

The number of healthy cells extracted from the aligned nanofiber device's aspirate was shown to be sufficient material for later genomic and transcriptomic analysis. A general continuity between the tumor bulk, aspirated sample, and adhered tissue inside the device has been established both with genomic and immunohistochemistry analyses (Figure 4 and Supplementary Figure 4). It was also shown that the device itself (with or without the nanofiber) does not have a significant effect on the brain tumors' immune profile and component cell ratio (Figure 4A–D). While the tumor and tumor immune microenvironment are both present inside aligned nanofiber device, future in-depth studies are needed to examine the spatial distribution of cells within the device in comparison to the primary tumor, as it might be possible that the aligned nanofiber device induces migration of the more invasive subtypes within the tumor.

In addition to concerted migration enabled by nanofibers, it is possible that the aligned nanofiber device partially facilitates initial proximal movement of cells, although limited, via some capillary effect. Devices with different polymer types and alignments could have different effects on the cells, inducing differential cell accumulation due to their different physical properties. However, our observations both in this study and previous studies (both in vitro and in vivo) indicate a very gradual and consistent migration within weeks and not hours, suggesting a capillary effect's role in inducing cell migration, if any, would be insignificant overall. The data presented here comparing PCL and PU aligned nanofiber materials supports the existing evidence that cell migration on aligned nanofibers is dependent perhaps more on the topography of the substrate than its composition (Figure 1A, Supplementary Figure 6). Moreover, PCL and PU aligned nanofiber materials did not differentially impact proliferation rate (Supplementary Figure 7).

Cell expansion data from aspirated fluid represented perhaps the most significant application of our aligned nanofiber devices: to provide culturable cells via minimally invasive extracortical access. While it was possible to culture cells obtained from the biopsy samples as a proof of concept, we understand that culturing human GBM

obtained from patients is prohibitively challenging.[43] And while neurospheres and organoids of individual human GBM patients would strengthen the translatability of our device, the scope of this study is limited to the demonstration of access to cellular content of GBM. Even without the option of culturing the biopsied human GBM samples, access to tissue and cells from in situ tumor would provide a plethora of useful information about the state and progression of the disease. In addition, as technology advances with the ability to culture cells obtained from patients in the fields of individualized medicine and immunotherapy, the aligned nanofiber device will be ideal to provide access to the tumor cells throughout the different stages of tumor progression.

The clinical benefit of monitoring specific biomarkers across multiple time periods has been further demonstrated in liquid biopsy studies.[10,32,33] One study utilizing liquid biopsy to analyze GBM's response to anti-VEGF therapy found that the circulating levels of VEGF following intervention decreased significantly,[44] establishing VEGF as an indicator of therapeutic efficacy. Similar information for additional markers could enable fine-tuning of treatment course, but it is still limited by the inherent shortcomings of liquid biopsy, including the lack of relevant information about tumor microenvironment. It is likely that direct assessment at the tumor site would allow for superior monitoring and consequently greater therapeutic benefit. For instance, a continuous biopsy platform could offer the ability to assess major fluctuations in GBM's immune microenvironment, mutational burden, and major mutations such EGFRvIII, BRAFV600E, TERT, and TP53.[26,45]

We hypothesize that frequent sampling may also have a role in distinguishing progression from pseudoprogression, a common MRI pattern that mimics tumor progression but not necessarily accompanied by clinical deterioration.[46] For example, assessing immune cell influx and biomarker composition around the tumor can provide insight into whether perceived cancer growth is merely a physiological reaction to treatment or true spread of the malignant tumor. Pseudoprogression often leads to premature withholding of adjuvant temozolomide or to overestimation of second-line therapy's efficacy, complicating accurate prognosis.[47] As a result, adjuvant temozolomide is typically continued for at least 3 months after therapy, regardless of findings on the first post-radiation evaluation.[47]

Additionally, due to the limited effectiveness of standard-of-care treatment options, there is substantial effort to enroll patients in clinical trials. However, the logistical burden associated with matching patients to trials that have the highest chance of success is significant.[48,49] Continuous access to GBM would reduce the time needed to screen and enroll patients in clinical trials and provide temporal feedback on trial effectiveness in an outpatient setting whenever clinicians deemed suitable.[23,24]

While the safety and functionality of this neural tract-inspired device for on-demand and facile sampling of GBM in these in vivo models were established, more extensive studies are needed to assess the device's specific interactions with the BBB and the effects of the device on the tumor microenvironment. Additionally, due to the inherent heterogeneity both within and between tumors, determination of the best placement for this device (as well as the number of devices implanted) is also critical and should be informed by clinical imaging and surgical guidance. The various limitations of the glioblastoma models used are also important to consider, with the limited migration capacity of U87MG cells being particularly relevant to this investigation. By using the F98-GFP+ model in parallel, the effects noticed are unlikely to be an artifact of one particular model system. Finally, while the potential for therapeutic benefit and clinical impact of this device have been established, a thorough clinical feasibility study is needed to ensure the safety and functionality of this approach.

Supplementary material

Supplementary material is available online at *Neuro-Oncology* (https://academic.oup.com/neuro-oncology).

Keywords

glioblastoma | on-demand biopsy | tumor microenvironment

Funding

This work was made possible by generous support from the Marcus Foundation.

Acknowledgments

We would like to thank Duke Center for In Vivo Microscopy (CIVM), particularly Dr. Stephanie Blocker and Dr. Allen Johnson for their expert support. We are grateful to Michelle Bowie and Aaron Briley for their input on genomic analysis methods and procedures. Furthermore, we thank Nicolas Devos, Wei Chen, and the Duke Sequencing and Genomic Technologies Shared Resource for their assistance with RNA and DNA sequencing and analysis, and Nadia Hossainy. We acknowledge David Corcoran and the Genomic Analysis and Bioinformatics Shared Resource for their consultation regarding genomic and transcriptomic data analysis. This work was made possible by generous support from the Marcus Foundation. Figures created with BioRender.com were referenced.

Conflict of Interest statement

S.M., B.B., R.B., and N.M. are licensing the aligned nanofiber technology discussed in this work to a private entity for translation and commercialization.

Authorship Statement

M.B.: Manuscript writing, experimental oversight, experimental design, implementation, analysis, and interpretation of data. A.C.: Manuscript writing, experimental oversight, experimental design, implementation, analysis, and interpretation of data. E.I.: Manuscript writing, execution, and analysis. N.M.: Manuscript writing, experimental design, implementation, analysis, and interpretation of data. S.M.: Manuscript writing, implementation, analysis, and interpretation of data. S.P.: Experimental design, implementation, and execution. S.K.: Experimental design, execution, and interpretation of data. K.S.: Manuscript writing, experimental oversight, and interpretation of data. B.B.: Manuscript writing, experimental design, experimental oversight, and interpretation of data. S.G.: Experimental design, experimental oversight, and interpretation of data. W.C.: Manuscript writing and interpretation of data. D.M.A.: Manuscript writing and experimental oversight. R.B.: Manuscript writing, experimental oversight, and experimental design. N.M.: Manuscript writing, experimental oversight, experimental design, implementation, analysis, and interpretation of data.

Data Availability

While the data supporting the finding can be found within the article and the supplementary materials, data presented here will be made available upon reasonable request in the form of PDF copies of raw data obtained and observations made during the study.

Affiliations

Department of Biomedical Engineering, Duke University, Durham, North Carolina, USA (A.C., E.I., N.M, S.M., S.P., R.B., N.M); Department of Neurosurgery, Emory University, Atlanta, Georgia, USA (M.I.B., B.B., N.M); Department of Neurosurgery, Duke University, Durham, North Carolina, USA (S.T.K., D.M.A.); Molecular Physiology Institute, Duke University, Durham, North Carolina, USA (K.S., S.G.); Department of Biology, Emory University, Atlanta, Georgia, USA (R.B.); Center for Genomic and Computational Biology, Duke University, Durham, Georgia, USA (W.C.)

References

1. Ambady P, Bettegowda C, Holdhoff M. Emerging methods for disease monitoring in malignant gliomas. *CNS Oncol.* 2013;2(6):511–522.
2. Neagu MR, Huang RY, Reardon DA, Wen PY. How treatment monitoring is influencing treatment decisions in glioblastomas. *Curr Treat Options Neurol.* 2015;17(4):15.
3. Weller M, Cloughesy T, Perry JR, Wick W. Standards of care for treatment of recurrent glioblastoma—are we there yet? *Neuro-Oncol.* 2013;15(1):4–27.
4. Verduin M, Compter I, Steijvers D, et al. Noninvasive glioblastoma testing: Multimodal approach to monitoring and predicting treatment response. *Dis Markers.* 2018;2018:1–11.
5. Boonzaier NR, Piccirillo SG, Watts C, Price SJ. Assessing and monitoring intratumor heterogeneity in glioblastoma: how far has multimodal imaging come? *CNS Oncol.* 2015;4(6):399–410.
6. Kan LK, Drummond K, Hunn M, et al. Potential biomarkers and challenges in glioma diagnosis, therapy and prognosis. *BMJ Neurol Open.* 2020;2(2):e000069.
7. Tan AC, Ashley DM, López GY, et al. Management of glioblastoma: state of the art and future directions. *CA Cancer J Clin.* 2020;70(4):299–312.
8. Nelson SJ, Cha S. Imaging glioblastoma multiforme. *Cancer J.* 2003;9(2):134–145.
9. Saenz-Antoñanzas A, Auzmendi-Iriarte J, Carrasco-Garcia E, et al. Liquid biopsy in glioblastoma: opportunities, applications and challenges. *Cancers.* 2019;11(7):950.
10. Sareen H, Garrett C, Lynch D, et al. The role of liquid biopsies in detecting molecular tumor biomarkers in brain cancer patients. *Cancers.* 2020;12(7):1831.
11. Gatto L, Franceschi E, Di Nunno V, et al. Liquid biopsy in glioblastoma management: From current research to future perspectives. *Oncologist.* 2021;26(10):865–878.
12. Shankar GM, Balaj L, Stott SL, Nahed B, Carter BS. Liquid biopsy for brain tumors. *Expert Rev Mol Diagn.* 2017;17(10):943–947.
13. Webinar: Stephen Bagley, MD - *Liquid Biopsy for Brain Tumors: Recent Advances and Future Directions - YouTube.* Available at https://www.youtube.com/watch?v=HVwdgevQrb0. Accessed August 16, 2021.
14. Chang K, Zhang B, Guo X, et al. Multimodal imaging patterns predict survival in recurrent glioblastoma patients treated with bevacizumab. *Neuro-Oncol.* 2016;18(12):1680–1687.
15. Department of Neurosurgery, Jordan University Hospital and Medical School, University of Jordan, Amman, Jordan, Tamimi AF, Juweid M, Department of Radiology and Nuclear Medicine, Jordan University Hospital and Medical School, University of Jordan, Amman, Jordan. Epidemiology and outcome of glioblastoma. In: Department of Neurosurgery, University Hospitals Leuven, Leuven, Belgium, De Vleeschouwer S, ed. *Glioblastoma.* Codon Publications; 2017:143-153.
16. Jain A, Betancur M, Patel GD, et al. Guiding intracortical brain tumour cells to an extracortical cytotoxic hydrogel using aligned polymeric nanofibres. *Nat Mater.* 2014;13(3):308–316.
17. Lövblad KO, Basssetti C. Diffusion-weighted magnetic resonance imaging in brain death. *Stroke.* 2000;31(2):539–542.
18. Cox M, Kung D, Hurst RW, Bagley LJ, Ali Nabavizadeh S. Significance of the absent vertebral artery T2 flow void on cervical spine MRI in atraumatic patients without acute neurological symptoms. *Neuroradiol J.* 2019;32(3):154–157.
19. Korbecki A, Zimny A, Podgórski P, Sąsiadek M, Bladowska J. Imaging of cerebrospinal fluid flow: fundamentals, techniques, and clinical applications of phase-contrast magnetic resonance imaging. *Polish J Radiol.* 2019;84:240–250.
20. Newton, H., *Handbook of Neuro-Oncology Neuroimaging.* Elsevier; 2016.
21. Wendels S, Avérous L. Biobased polyurethanes for biomedical applications. *Bioact Mater.* 2021;6(4):1083–1106.
22. Steen CB, Liu CL, Alizadeh AA, Newman AM. Profiling cell type abundance and expression in bulk tissues with CIBERSORTx. *Methods Mol Biol (Clifton, N.J.).* 2020;2117:135–157.
23. Singh K, Hotchkiss KM, Parney IF, et al. Correcting the drug development paradigm for glioblastoma requires serial tissue sampling. *Nat Med.* 2023;29(10):2402–2405.
24. Nduom EK, Gephart MH, Chheda MG, et al. Re-evaluating biopsy for recurrent glioblastoma: a position statement by the Christopher Davidson forum investigators. *Neurosurgery.* 2021;89(1):129–132.

25. Lynes J, Jackson S, Sanchez V, et al. Cytokine microdialysis for real-time immune monitoring in glioblastoma patients undergoing checkpoint blockade. *Neurosurgery*. 2019;84(4):945–953.
26. Touat M, Li YY, Boynton AN, et al. Mechanisms and therapeutic implications of hypermutation in gliomas. *Nature*. 2020;580(7804):517–523.
27. Lynes JP, Nwankwo AK, Sur HP, et al. Biomarkers for immunotherapy for treatment of glioblastoma. *J ImmunoTher Cancer*. 2020;8(1):e000348.
28. Cunnea P, Gorgy T, Petkos K, et al. Clinical value of bioelectrical properties of cancerous tissue in advanced epithelial ovarian cancer patients. *Sci Rep*. 2018;8(1):1–12.
29. Cunnea P, Gowers S, Moore JE, et al. Review article: novel technologies in the treatment and monitoring of advanced and relapsed epithelial ovarian cancer. *Converg Sci Phys Oncol*. 2017;3(1):013002.
30. Saenz-Antoñanzas A, Auzmendi-Iriarte J, Carrasco-Garcia E, et al. Liquid biopsy in glioblastoma: opportunities. *Cancers*. 2019;11(950):1–20.
31. Klekner A, Szivos L, Virga J, et al. Significance of liquid biopsy in glioblastoma—a review. *J Biotechnol*. 2019;298:82–87.
32. Ko J, Baldassano SN, Loh PL, et al. Machine learning to detect signatures of disease in liquid biopsies—a user's guide. *Lab Chip*. 2018;18(3):395–405.
33. Rincon-Torroella J, Khela H, Bettegowda A, Bettegowda C. Biomarkers and focused ultrasound: the future of liquid biopsy for brain tumor patients. *J Neurooncol*. 2022;156(1):33–48.
34. Nduom EK, Glod J, Brown DA, et al. Clinical protocol: feasibility of evaluating abemaciclib neuropharmacokinetics of diffuse midline glioma using intratumoral microdialysis. Burger MC, ed. *PLoS One*. 2023;18(9):e0291068.
35. Thelin EP, Nelson DW, Ghatan PH, Bellander BM. Microdialysis monitoring of CSF parameters in severe traumatic brain injury patients: a novel approach. *Front Neurol*. 2014;5:159.
36. Sun H, Mei L, Song C, Cui X, Wang P. The in vivo degradation, absorption and excretion of PCL-based implant. *Biomaterials*. 2006;27(9):1735–1740.
37. Ma DW, Zhu R, Wang YY, Zhang ZR, Wang XY. Evaluation on biocompatibility of biomedical polyurethanes with different hard segment contents. *Front Mater Sci*. 2015;9(4):397–404.
38. Rusu LC, Ardelean LC, Jitariu AA, Miu CA, Streian CG. An insight into the structural diversity and clinical applicability of polyurethanes in biomedicine. *Polymers*. 2020;12(5):1197.
39. Uscátegui YL, Díaz LE, Valero MF. In vitro and in vivo biocompatibility of polyurethanes synthesized with castor oil polyols for biomedical devices. *J Mater Res*. 2019;34(4):519–531.
40. Huang YJ, Hung KC, Hsieh FY, Hsu S. Carboxyl-functionalized polyurethane nanoparticles with immunosuppressive properties as a new type of anti-inflammatory platform. *Nanoscale*. 2015;7(48):20352–20364.
41. Huang APH, Lai DM, Hsu YH, et al. An anti-inflammatory gelatin hemostatic agent with biodegradable polyurethane nanoparticles for vulnerable brain tissue. *Mater Sci. Eng. C, Mater Biol Appl*. 2021;121:111799.
42. Rangwala HS, Ionita CN, Rudin S, Baier RE. Partially polyurethane-covered stent for cerebral aneurysm treatment. *J Biomed Mater Res B Appl Biomater*. 2009;89B(2):415–429.
43. Xie Y, Bergström T, Jiang Y, et al. The human glioblastoma cell culture resource: Validated cell models representing all molecular subtypes. *EBioMedicine*. 2015;2(10):1351–1363.
44. Groot JF de, Piao Y, Tran H, et al. Myeloid biomarkers associated with glioblastoma response to anti-vascular endothelial growth factor therapy with aflibercept. *Clin Cancer Res Off J Am Assoc Cancer Res*. 2011;17(14):4872.
45. Johnson BE, Mazor T, Hong C, et al. Mutational analysis reveals the origin and therapy-driven evolution of recurrent glioma. *Science*. 2014;343(6167):189–193.
46. Balaña C, Capellades J, Pineda E, et al; GLIOCAT Group. Pseudoprogression as an adverse event of glioblastoma therapy. *Cancer Med*. 2017;6(12):2858–2866.
47. Jia W, Gao Q, Han A, Zhu H, Yu J. The potential mechanism, recognition and clinical significance of tumor pseudoprogression after immunotherapy. *Cancer Biol Med*. 2019;16(4):655–670.
48. Lee EQ, Chukwueke UN, Hervey-Jumper SL, et al. Barriers to accrual and enrollment in brain tumor trials. *Neuro-Oncol*. 2019;21(9):1100–1117.
49. Zanders ED, Svensson F, Bailey DS. Therapy for glioblastoma: is it working? *Drug Discov Today*. 2019;24(5):1193–1201.